Measurement of the charge asymmetry in the decay $K_L^0 \to \pi^\pm \mu^\mp \nu$ [†]

R. Piccioni, G. Donaldson, D. Fryberger, D. Hitlin, J. Liu, B. Meyer,[‡] A. Rothenberg,[§] M. Schwartz,
D. Uggla, and S. Wojcicki[||]

Physics Department and Stanford Linear Accelerator Center, Stanford University, Stanford, California 94305

D. Dorfan[||]

Physics Department, University of California, Santa Cruz, California 95064

R. Messner

Duane Physical Laboratories, University of Colorado, Boulder, Colorado 80302

(Received 12 November 1973)

The charge asymmetry in the decay $K_L^0 \to \pi^\pm \mu^\mp \nu$ has been measured to be $(2.78 \pm 0.51) \times 10^{-3}$, leading to a value of $\mathrm{Re}\,\epsilon$ in good agreement with the results from the $K_L^0 \to 2\pi$ decay modes.

I. INTRODUCTION

The observation of a charge asymmetry in the decay $K_L^0 \to \pi^\pm l^\mp \nu$ is direct evidence of CP violation. We present here a detailed account of a recent measurement[1] of the charge asymmetry in 7.7 $\times 10^6$ $K_L^0 \to \pi^\pm \mu^\mp \nu$ events obtained with the K^0 spectrometer facility at the Stanford Linear Accelerator Center. The following paper, hereafter referred to as paper II, presents a detailed discussion of an analysis of a part of these data to extract the form factors of the decay.

II. CP PHENOMENOLOGY

If we write the states of the K^0-$\overline{K}^0$ system which have definite lifetime as

$$|K_S^0\rangle = \frac{1}{[2(1+|\epsilon|^2)]^{1/2}}\left[(1+\epsilon)|K^0\rangle + (1-\epsilon)|\overline{K}^0\rangle\right],$$

$$|K_L^0\rangle = \frac{1}{[2(1+|\epsilon|^2)]^{1/2}}\left[(1+\epsilon)|K^0\rangle - (1-\epsilon)|\overline{K}^0\rangle\right],$$

the nonorthogonality of the long- and short-lived states, $\langle K_S^0 | K_L^0 \rangle = 2\mathrm{Re}\,\epsilon$, may be directly obtained by a measurement of the difference in the decay rates to CP-conjugate leptonic modes.

With the assumption of CPT invariance, we may define the K_{l3}^0 decay amplitudes as

$$\langle \pi^- l^+ \nu | H_{\mathrm{wk}} | K^0 \rangle$$
$$\propto \psi_{l^+}^\dagger \gamma^\lambda (1+\gamma_5)\psi_\nu \left[f_+(p_{K^0}+p_{\pi^-})_\lambda + f_-(p_{K^0}-p_{\pi^-})_\lambda\right],$$

$$\langle \pi^+ l^- \overline{\nu} | H_{\mathrm{wk}} | \overline{K}^0 \rangle$$
$$\propto \psi_{l^-}^\dagger \gamma^\lambda (1+\gamma_5)\psi_{\overline{\nu}} \left[f_+^*(p_{\overline{K}^0}+p_{\pi^+})_\lambda + f_-^*(p_{\overline{K}^0}-p_{\pi^+})_\lambda\right],$$

$$\langle \pi^- l^+ \nu | H_{\mathrm{wk}} | \overline{K}^0 \rangle$$
$$\propto \psi_{l^+}^\dagger \gamma^\lambda (1+\gamma_5)\psi_\nu \left[g_+(p_{\overline{K}^0}+p_{\pi^-})_\lambda + g_-(p_{\overline{K}^0}-p_{\pi^-})_\lambda\right],$$

$$\langle \pi^+ l^- \overline{\nu} | H_{\mathrm{wk}} | K^0 \rangle$$
$$\propto \psi_{l^-}^\dagger \gamma^\lambda (1+\gamma_5)\psi_{\overline{\nu}} \left[g_+^*(p_{K^0}+p_{\pi^+})_\lambda + g_-^*(p_{K^0}-p_{\pi^+})_\lambda\right],$$

where f and g are the complex $\Delta S = +\Delta Q$ and $\Delta S = -\Delta Q$ amplitudes, respectively. If we define $x_+ = f/g$ and $x_- \equiv x_+^* = f^*/g^*$, then the decay rates $\Gamma_\pm = \mathrm{Rate}\,(K_L^0 \to \pi^\mp l^\pm \nu)$ may be written as

$$\Gamma_\pm \propto (1+|\epsilon|^2)(1+|\overline{x}_\pm|^2)$$
$$\pm 2\mathrm{Re}\,\epsilon(1-|\overline{x}_\pm|^2) - 2(1-|\epsilon|^2)\mathrm{Re}\,\overline{x}_\pm$$
$$+ 4\,\mathrm{Im}\,\epsilon\,\mathrm{Im}\,\overline{x}_\pm ,$$

where $\overline{x}_\pm$ represent the appropriate average values for $x_\pm$.

If we define the charge asymmetry by $\delta = (\Gamma_+ - \Gamma_-)/(\Gamma_+ + \Gamma_-)$, then to first order in ϵ and $\overline{x}_\pm$

$$\delta = 2\mathrm{Re}\,\epsilon \frac{2 - |\overline{x}_+|^2 - |\overline{x}_-|^2}{2 + |\overline{x}_+|^2 + |\overline{x}_-|^2 - 2(\mathrm{Re}\,\overline{x}_+ + \mathrm{Re}\,\overline{x}_-)}$$

or

$$\delta = 2\mathrm{Re}\,\epsilon \frac{1 - |x|^2}{|1-x|^2} ,$$

where $x = \overline{x}_+$. In this limit, the charge asymmetry is constant across the Dalitz plot, regardless of any $t = (p_K - p_\pi)^2$ dependence of the form factors associated with the amplitudes. On the other hand, in the presence of T violation, interference and final-state effects may cause the charge asymmetry to vary as a function of the Dalitz plot position.[2] Nevertheless, to the extent that $\Delta S = -\Delta Q$ amplitudes may be neglected, a measurement of the charge asymmetry in K_{l3}^0 decays provides a direct measurement of the nonorthogonality of the K_L^0 and K_S^0 eigenstates.

III. EXPERIMENTAL SETUP

The experiment was performed at the Stanford Linear Accelerator Center (SLAC), where we studied K_L^0 decays in a neutral beam of well-defined direction and time structure. Charged particles emerging from this beam were detected by

arrays of scintillation counters and wire spark chambers, positioned on both sides of a dipole analyzing magnet. In addition, counter hodoscopes placed behind a lead wall were used to identify muons. Acquisition logic gathered and condensed the information from the detectors and transferred it to an on-line computer, which recorded the data on magnetic tape for later analysis.

We now consider each aspect of the setup in detail.

A. Beam

The layout of beam line 8 in end station B at SLAC is shown in Fig. 1. A secondary beam was taken through a hole in a 6-m-thick shielding block, at an angle of 50 mrad to a primary beam of 19-GeV electrons incident on a 30-cm beryllium target. A total of 20 cm of lead and 168 cm of polyethylene were placed in the path of this secondary beam to remove photons and reduce the neutron to K_L^0 ratio, respectively. The beam-defining collimator was placed 11.5 m downbeam of the production target. Along the subsequent flight path in air to the detectors, additional shielding was placed around the beam and three sweeping magnets were used to bend charged particles out of the beam. Two other collimators were used to remove scattered particles, but did not intersect the beam itself. The beam cross section at the center of the spectrometer magnet $8D4$, 78.6 m from the target, was 69 cm wide by 33 cm high.

The principal components of this neutral beam were K^0's and neutrons. Although the neutron flux was dominant at low momenta (< 2 GeV/c), it was equal to the K_L^0 flux at about 4 GeV/c, and dropped off more sharply than the K_L^0 flux at high momenta.[3] The K_L^0 decay momentum spectrum, as observed in this experiment, is shown in Fig. 2. A full description of how this spectrum was obtained is given in paper II.

Under normal running conditions, we received 160 pulses per second, each of 1600 nsec duration. Each pulse was divided into buckets of < 20 psec duration, with 12.5 nsec between buckets. A signal induced in a coaxial cable placed immediately downbeam of the target enabled us to determine the kaon production time. With this CABLE pulse and the arrival time of the kaon charged decay products, we were able to determine the momentum of the kaon in the laboratory.

B. Counters and trigger logic

The experimental apparatus is shown in Fig. 3. There were five scintillation counter banks: V, T, A, B, and C. The decay volume, which was filled with helium to reduce beam interactions, was defined to be the region between the V and T counter banks. The single V counter, 107 cm $\times 46$ cm $\times 0.64$ cm, was viewed by two 56AVP phototubes at each end, and served as a veto counter. The T counter bank was placed immediately before the front wire chambers and consisted of two vertical rows of 20 scintillators each, 0.32 cm thick, covering a total area 102 cm by 122 cm. Each T counter was viewed by a single 56AVP phototube. The 12 A counters, each 1 cm thick, were arranged vertically behind the rear wire chambers, and had an active area of 183 cm $\times 122$ cm. Behind the first and second sections of the lead wall were the 14 B and 16 C counters, respectively. These
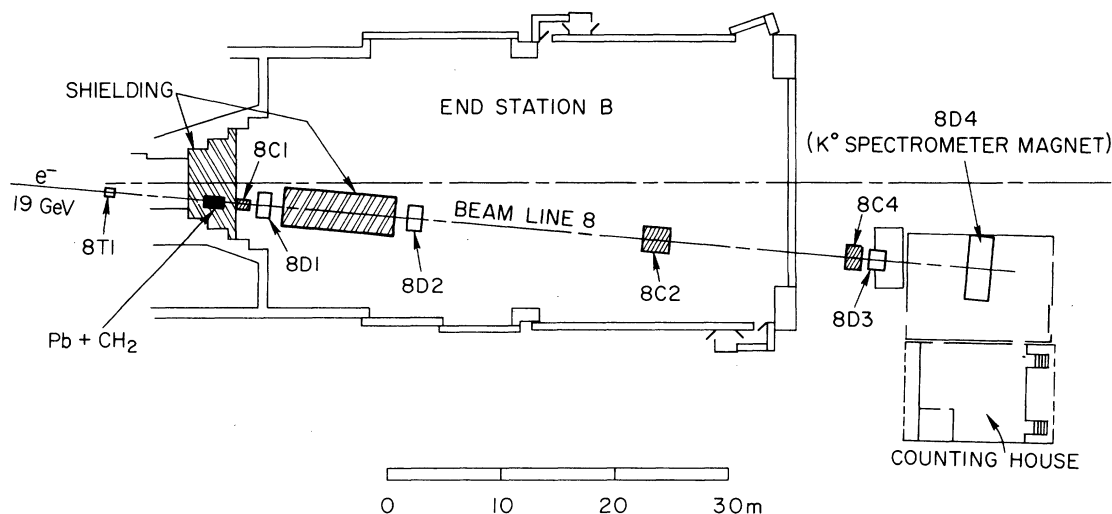

FIG. 1. Arrangement of beam line 8 in end station B at SLAC. The production target is shown as $8T1$, while the beam-defining collimator is $8C1$. $8C2$ and $8C4$ are two other beam collimators, while $8D1$, $8D2$, and $8D3$ are the sweeping magnets.
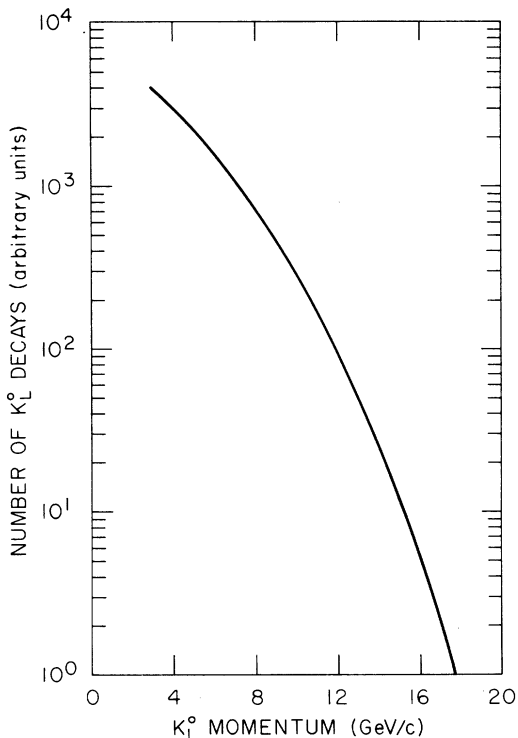
FIG. 2. K_L^0 decay momentum spectrum as observed in this experiment. For details of how this spectrum was obtained, see the section on MONTE CARLO in paper II.

56AVP.'s, while those on the A counters were XP1021's for superior time resolution. A timing analog-to-digital converter (ADC) unit was used on each A phototube, and on pairs of nonadjacent phototubes in both the B and C counter banks. The TOF resolution, as shown in Fig. 4, was determined by studying $K_S^0 \to \pi^+\pi^-$ events in a regenerator run to be $\pm\frac{1}{3}$ nsec over a flight path of some 75 m. The pulse heights in the A, B, and C counters were also recorded with each event.

The T and A counters were closest to the spectrometer magnet, in a fringe field that did not exceed 15 gauss. Their phototubes were protected by two concentric magnetic shields, the inner one made of Molypermalloy and the outer made of iron. Since the B and C counters were 380 and 450 cm from the magnetic mirrors, respectively, in a field of 2–3 gauss, the Molypermalloy shields alone were sufficient. The shielding was such that reversing the field of the spectrometer magnet was observed to have little effect on the pulse height of any individual counter (Sec. VII H).

The logic signature for $K_{\mu 3}^0$ events was $\bar{V}\cdot 2T\cdot A\cdot B\cdot C\cdot$CABLE. When such a trigger was satisfied, latch units recorded which counters had fired, and the ADC's recorded the times and pulse heights observed in each A, B, and C phototube.

C. Wire chambers and acquisition logic

Two 10-gap wire spark chambers[4] were placed on opposite sides of the spectrometer magnet. Each gap measured spark positions with respect to one coordinate direction, and each group of 10 gaps consisted of 4 X's, 4 Y's, 1 U, and 1 V (Z was the beam direction, X horizontal, Y vertical, U and V two other directions in the XY plane). The

were each 1.27 cm thick, positioned vertically to cover areas 214 cm $\times$ 168 cm and 244 cm $\times$ 168 cm, respectively.

Time-of-flight (TOF) measurements were made with the A, B, and C counters, which were each viewed by two phototubes, one at each end. The phototubes used on the B and C counters were
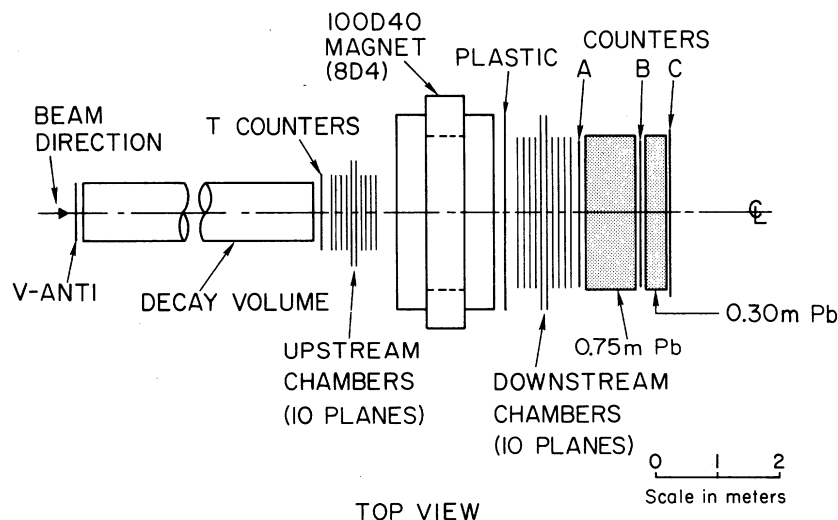

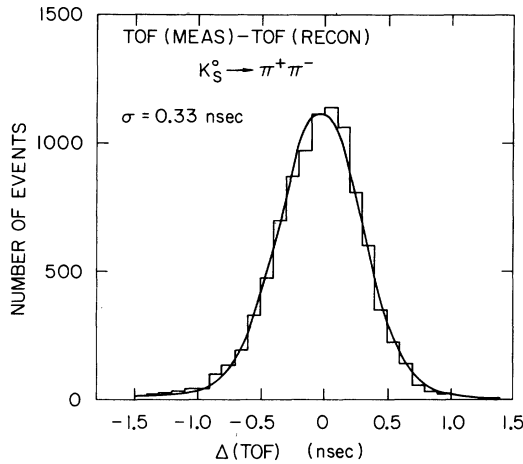FIG. 3. SLAC K^0 spectrometer—plan view of the experimental apparatus.

FIG. 4. The time-of-flight resolution as obtained from $K^0_S \rightarrow \pi^+\pi^-$ decays following a copper regenerator.

wires in the front U and V planes were at $+45°$ and $-45°$ with respect to the X axis, while those in the rear U and V planes were at $+30°$ and $-60°$ relative to the X axis, respectively. The dimensions of the upbeam and downbeam X and Y chambers were $1.2 \text{ m} \times 1.2 \text{ m}$ and $2.4 \text{ m} \times 1.2 \text{ m}$, respectively. There were a total of 30 000 readout wires; the wire spacing was 1 mm and the wire diameter was 0.1 mm. The use of 10 gaps to determine three-dimensional line segments provided a high degree of redundancy, which enabled us to isolate tracks of interest even in the presence of considerable background and occasional inefficiency in individual gaps.

A 1-nF capacitor was connected to each wire in the wire-chamber array. When the chambers were fired, each spark deposited charge on one or more of these capacitors, depending on the width of the spark. Acquisition logic subsequently interrogated these capacitors and transmitted the locations of those which were charged to the on-line computer. This readout system was unaffected by magnetic fields, and had the capability of handling many sparks per wire-chamber plane.

D. Spectrometer magnet

The spectrometer magnet had a gap of 2.5 m $\times 1 \text{ m} \times 1$ m which was filled with a helium bag. Magnetic mirrors were attached to both sides of the magnet to reduce the fringe fields. The experiment was run with a magnetic field integral of 12.6 kGm, corresponding to $\Delta P_{\perp} = 0.377$ GeV/c. This field, together with the resolution of the wire chambers, gave a momentum resolution of $\pm 1\%$ for 2.7-GeV/c charged tracks. The vertical component of the field at the center of the lower pole face was continuously monitored with an NMR probe. The value of this NMR reading was re-

corded at the beginning of each data run and remained constant to $\pm 0.1\%$ throughout the experiment.

The three components of the magnetic field were measured at 36 000 points within the field region in a 10 cm $\times 2.5$ cm $\times 2.5$ cm grid. Line integrals $\int B_Y dZ$ were also taken through the magnet at each point in a 10 cm $\times 2.5$ cm grid in the XY plane, and these were found to be consistent with the grid point measurements.

E. Lead wall

The lead wall was divided into two sections: The first was 75 cm thick and the second was 30 cm thick, for a total of 7.7 interaction lengths. Initially, we observed a spray of low-energy neutrons produced by beam interactions in the lead wall, resulting in high accidental counting rates in the A, B, and C counter banks. This problem was alleviated by placing paraffin slabs between these counter banks and the lead wall.

The minimum energy required for a muon to traverse the 8.7 interaction lengths of lead and paraffin which made up the muon filter was 1.6 GeV.

F. On-line computer

The on-line computer system consisted of a PDP-9 with 24K of core, a teletype, three DEC-tape drives, two magnetic tape drives, and a display scope. Its primary function was to record the data, which entered the computer via a DMA port,[4] onto magnetic tapes for later analysis. It also ran periodic diagnostics on various elements of the apparatus, and updated histograms of counter and wire-chamber data, thereby enabling the experimenter to spot equipment malfunctions rapidly.

IV. DATA COLLECTION

Data runs lasted approximately two hours. After every other run, the polarity of the spectrometer magnet was reversed and various diagnostics and calibrations were run. The latter included a complete test of the readout electronics, monitoring of all phototube high voltages, and pulser and muon runs which calibrated the ADC units, as discussed below.

A. Pulser runs

Each scintillation counter had a photodiode imbedded in it. A pulser run consisted of the computer selecting various combinations of counters and repeatedly pulsing their photodiodes, thus generating artificial triggers. In this way the computer could readily locate malfunctioning phototubes, trigger logic units, or data-acquisition

logic units.

During data runs, the CABLE pulse provided a reference time for the ADC units, but during pulser runs, this reference time was provided by the pulser which activated the photodiodes. Midway through each pulser run, the computer switched in a delay of 7 nsec in this reference time. The resulting shift in the timing ADC reading for an individual counter determined the slope for its corresponding ADC unit. The average slope of the TOF ADC units used in the experiment was 0.135 nsec/channel.

B. Muon runs

By turning off the three beam sweeping magnets and setting the trigger requirement to $V \cdot T \cdot A \cdot B \cdot C \cdot$ CABLE, the arrival time of direct, $v \simeq c$ muons from the target was measured in each counter. This determined one additive constant for each phototube, so that all TOFs recorded in the data could be computed with respect to a common reference time.

V. DATA ANALYSIS

The raw data from the experiment consisted of 470 magnetic tapes containing 75 billion bits of uncorrelated spark and raw ADC information. The first stage of the analysis (PASS-1) reconstructed tracks in the front and rear chambers, in addition to calibrating the ADC units. The second stage (PASS-2) matched the front and rear tracks through the magnet, computed particle charge and momenta, identified muons, and found decay vertices. About 85% of all events passed this 2-stage analysis, which required 300 hours of IBM 360/91 time and condensed the raw data to 6.3 billion bits on 17 magnetic tapes. The final step of the analysis (PASS-3) consisted of selecting and categorizing these events in order to obtain the final data sample, and in order to study systematic biases.

A. Wire-chamber reconstruction

The most time-consuming phase of the analysis was the correlation of sparks to form tracks in PASS-1. Consider the extraction of X line segments from the upbeam set of 4 X planes. Our objective was to find all straight lines in the X projection which were formed by three or four sparks. Using every combination of a spark in plane $X1$ with a spark in plane $X3$, the line joining these two sparks was projected onto planes $X2$ and $X4$. If a spark was found within ± 4 wires of the projected X position on either or both of these planes, then an X line segment was found. The procedure was repeated, starting with pairs of sparks in planes

$X2$ and $X4$, and projecting onto planes $X1$ and $X3$. Any given spark was allowed to be part of several different line segments. For each X line segment that was found, a best-fit slope, intercept, and χ^2 were computed, the latter based on the distance between each spark on the line segment from the best-fit line through all the sparks on that line.

The set of X line segments, extracted by the above procedure, was found to contain a number of accidental lines, formed by combinations of sparks which did not represent true particle tracks. Under our normal running conditions, we expected to find 4.5 accidental 3-spark lines in the set of four X planes. In a procedure designed to discriminate against accidental lines, whenever two lines shared a common spark a penalty of nine units was added to the χ^2 of the line with the poorer χ^2. Similarly, lines formed with only three sparks were also given a χ^2 penalty of nine units. Finally, only lines with $\chi^2 < 14$ were accepted.

Having found all the X line segments in the front chambers, we applied the same procedure to find all the Y line segments. In order to determine which X and Y lines were related, each X and Y line segment was then projected onto the U plane. Since the U direction was a linear combination of X and Y, the expected spark position on the U plane could be computed for each pair of X and Y line segments. The same procedure was repeated for the V plane. If a spark was observed within ± 4 wires of the expected position in either the U or V plane, a complete track had been found. A χ^2 for the UV line segment was computed, and a penalty of nine units was added if either the U or V spark was missing. This UV χ^2 term was then added to the sum of the χ^2 for the X and Y line segments to form an over-all χ^2 for the complete track. This distribution is shown in Fig. 5. No cut was made on this over-all χ^2 term.
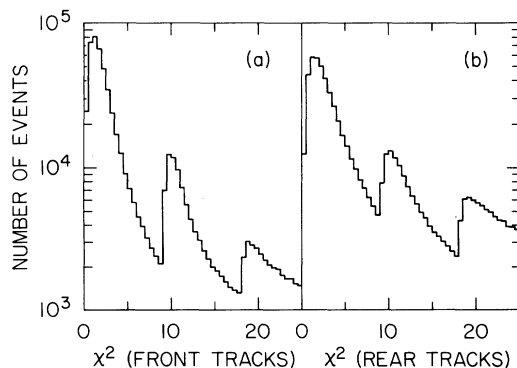
An identical analysis was used for the downbeam

FIG. 5. The distributions in the sum of X, Y, and UV line segment χ^2 terms for (a) front and (b) rear tracks in a sample of the data.

wire-chamber data, and the results of the track-finding analysis for each event were written onto an output tape in terms of the slope, intercept, and χ^2 for each front or rear track that was found. The standard deviation of a spark from the best-fit line was observed to be 0.35 mm, corresponding to an angular resolution for a charged track of ± 1 mrad. With a clearing field of 50 V/cm and a fringing field of ~50 gauss, the $\vec{E} \times \vec{B}$ effects were completely negligible and no corrections were needed.

The entire track-finding procedure was implemented so that the computer time required per event varied linearly with the number of sparks per wire-chamber plane.

B. Counter data and TOF calibration

The measured TOF for any individual A, B, or C counter was the average of the two times observed in the phototubes at each end. The vertical (Y) position information was obtained from the difference of these times divided by the velocity of light in the counter. This latter quantity was determined by comparing the Y information from timing in the A counters and the Y information obtained by extrapolating the rear tracks to the plane of the A counters. It was assumed to be constant in the A, B, and C counter banks. Each counter which triggered was given a latch assignment LAT = 1, as opposed to LAT = 0 for those which did not. When both B or C phototubes connected to the same ADC unit triggered in an event, the TOF and Y information in the corresponding counters were lost and this difficulty was noted by assigning LAT = 2 to those counters. Similarly, any counter with an unphysical TOF reading, corresponding to events from the previous or following beam buckets, was assigned LAT = 2.

The pulser runs and muon runs, as discussed in Sec. IV, determined the constants necessary to convert individual ADC readings into times measured with respect to a common reference point. We required only one more additive constant to make our measured times correspond to true TOFs. This final constant was determined by fitting the data to the $K^0_{\mu 3}$ hypothesis.

With the assumption that the observed charged tracks were from $K^0_L \to \pi \mu \nu$ decay, and computing the direction of the K^0_L from the target position and the decay vertex, the momentum of the kaon, and subsequently its TOF, may be calculated from the measured pion and muon momenta for any given event. However, since only the magnitude of the longitudinal component of the neutrino momentum could be calculated but not its direction, there was a quadratic ambiguity resulting in two solutions for the TOF. There were, however, a good number of events in which the difference between the two TOF solutions was less than 0.1 nsec. By comparing the average of the two solutions with the measured TOF for this special class of events, it was possible to determine the final additive constant.

The latch, TOF, Y position, and pulse-height information were also written on the PASS-1 output tape for each event.

C. Track matching through the magnet

The second stage of the analysis program, PASS-2, read the track and counter summary for each event of the PASS-1 output tape and began by matching the front and rear tracks through the magnet. The horizontal momentum transfer imparted to a charged track traversing the spectrometer magnet was virtually independent of the trajectory of the particle. For each particle candidate, defined as a combination of an upbeam and a downbeam track, an approximate momentum was computed from the horizontal bend angle:

$$P_0 = \frac{\Delta P_\perp (B_{\text{run}}/B_{\text{ref}})}{\alpha_r - \alpha_f} \; ,$$

where $\Delta P_\perp = 0.377$ GeV/c was the reference transverse momentum kick, B_{run} was equal to the value of the NMR reading for that particular data run, B_{ref} was equal to the reference NMR reading, and α_f and α_r were the observed X directional cosines for the front and rear tracks, respectively. Vertical-focusing corrections were then applied to the observed Y directional cosines of these tracks. Particle candidates were rejected if the corrected vertical bend angle was too large, or if the corrected front and rear segments did not cross satisfactorily in the magnet gap. Next, using the approximate momentum and the magnetic field measurements, the upbeam trajectory was integrated through the magnet to the downbeam chambers. Both the position and direction of this projected track were then compared with the corresponding observed values for the downbeam track. If both comparisons were satisfactory, the particle candidate was accepted and its momentum was refined:

$$P = P_0 \, \frac{\alpha_r(\text{proj}) - \alpha_f}{\alpha_r - \alpha_f} \; ,$$

where $\alpha_r(\text{proj})$ refers to the projected rear X directional cosine. Figure 6 shows the geometrical fits obtained for matching front and rear tracks in a sample of the data.

D. Muon identification

In the muon identification routine, we endeavored to find all possible muons that were recorded in
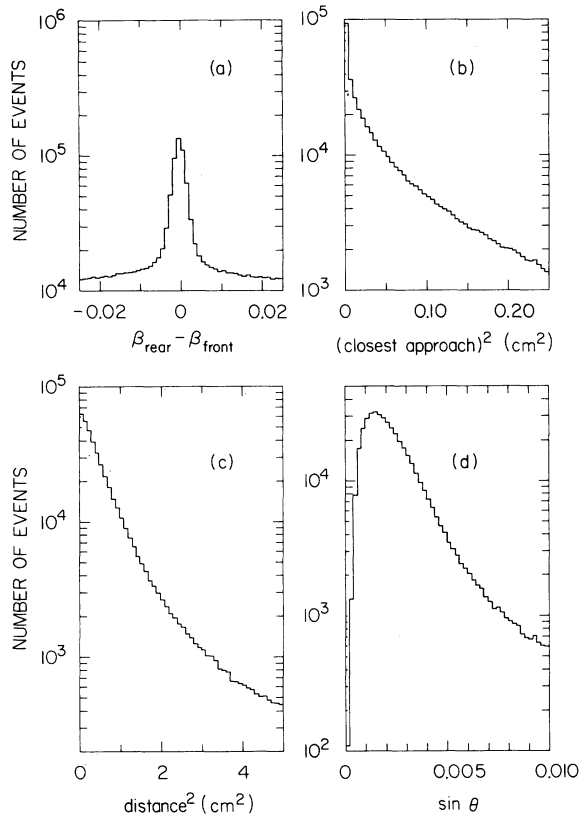
FIG. 6. Distributions in the variables associated with the matching of front and rear tracks through the spectrometer magnet: (a) $\beta_{\text{rear}} - \beta_{\text{front}}$ after vertical-focusing corrections, where β is the Y directional cosine (a cut was made at ± 0.025); (b) square of the distance of closest approach when both tracks were projected toward the center of the magnet (a cut was made at 50 cm^2); (c) square of the distance between the observed and projected positions of the rear track at the position of the rear U chamber (a cut was made at 50 cm^2); (d) sine of the angle between the observed and projected rear tracks at the position of the rear U chamber (a cut was made at 0.02).

the data. To achieve this, very liberal initial cuts were imposed and a muon χ^2 was assigned to each muon candidate. In this way, all possible muon candidates in each event would be passed on to the final stage of the muon analysis, where the best muon candidate(s) were kept on the basis of the χ^2.

Muons were identified by their ability to penetrate the lead wall. Each observed particle track which triggered an A counter was kept as a muon candidate if there was a B counter within ± 45 cm, and a C counter within ± 68 cm of the projected horizontal coordinate of the track at the B and C counter banks, respectively. These cuts were very loose, corresponding to $> \pm 4\sigma$. All possible combinations of latched B and C counters within

these limits were used. The distributions in $(X_{\text{proj}} - X_{\text{cen}})_{B/C}$, where X_{proj} represents the projected X, and X_{cen} the center of the B/C counter in question, are shown in Fig. 7.

The Y positions obtained from the timing information in the A, B, and C counters were then compared with those obtained by extrapolating the rear track to the corresponding counter bank. The quality of these Y comparisons is also shown in Fig. 7. The difference between the observed and projected Y position at the A counter was required to be within ± 17.5 cm, or about $\pm 4\sigma$. In order to account for the increase in multiple scattering with decreasing muon energy, the cuts imposed on the Y difference in the B and C counter banks were $\pm 20(1 + 1/E_\mu)$ cm and $\pm 37.5(1 + 1/E_\mu)$ cm, respectively, where E_μ denotes the energy of the muon as determined by the momentum measurement. These cuts corresponded to approximately $\pm 4\sigma$ for the average muon energy of 3.2 GeV.

The TOF's measured in the A, B, and C counters were then compared with one another after corrections were made to the B and C times for TOF shifts introduced by the multiple scattering and the slowing down of the muon in the lead. The observed differences in $|T_A - T_B|$, $|T_A - T_C|$, and $|T_B - T_C|$ were required to be within ± 2.5 nsec, or about $\pm 4\sigma$. These timing comparisons are shown in Fig. 8. The muon ionization energy
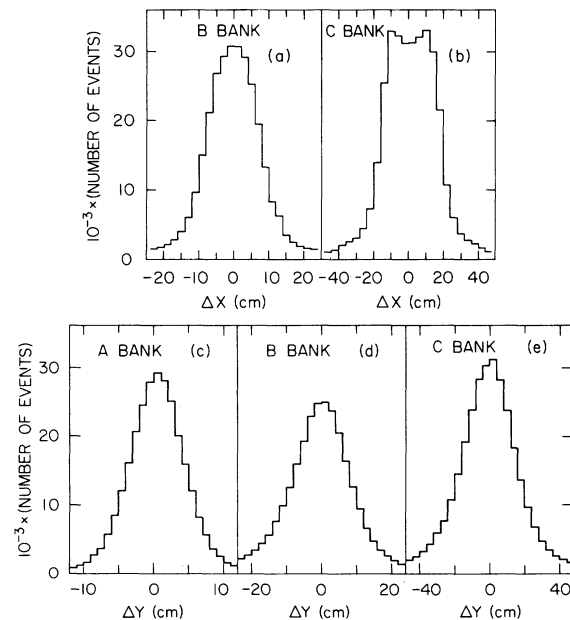

FIG. 7. Horizontal displacement between the projected X position of the muon track and the center of the associated counter in the (a) B and (b) C counter planes. Vertical displacement between the projected Y position of the muon track and the Y position as obtained from timing for the (c) A, (d) B, and (e) C counter banks.
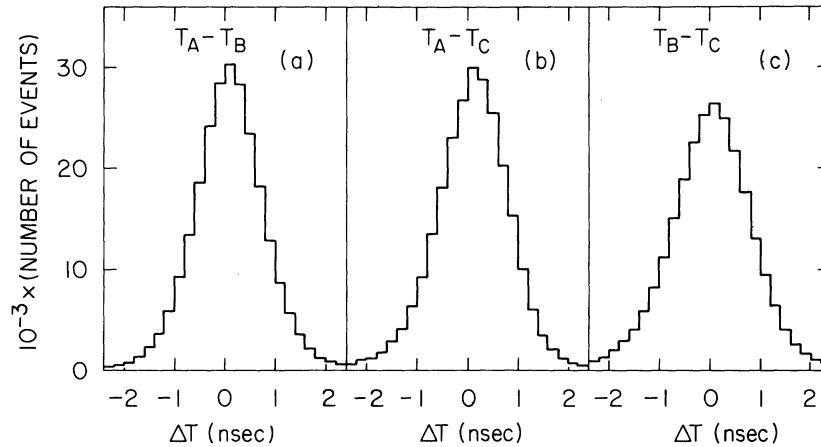
FIG. 8. Difference in the corrected muon TOF information between the (a) A and B, (b) A and C, and (c) B and C counter banks.

loss through each segment of the lead wall was calculated using the known path of the muon and an average dE/dX based on the measured incident energy and estimated final energy of the muon. Since this was only a rough estimate, all muons with a kinetic energy > -250 MeV at the C counter bank were kept at this stage of the analysis.

A muon χ^2 was then formed for each muon candidate:

$$\chi^2 = \left(\frac{\Delta X_B}{\sigma_{X_B}}\right)^2 + \left(\frac{\Delta X_C}{\sigma_{X_C}}\right)^2 + \left(\frac{\Delta Y_A}{\sigma_{Y_A}}\right)^2 + \left(\frac{\Delta Y_B}{\sigma_{Y_B}}\right)^2$$

$$+ \left(\frac{\Delta Y_C}{\sigma_{Y_C}}\right)^2 + \left(\frac{\Delta T_{AB}}{\sigma_{T_{AB}}}\right)^2 + \left(\frac{\Delta T_{BC}}{\sigma_{T_{BC}}}\right)^2 ,$$

where $\Delta T_{AB} = |T_A - T_B|$, etc. The errors used in computing the χ^2 term were on the average 25% larger than those determined from the experimental distributions described above. In a small number of cases where the TOF and Y information from one of the three counters was unreliable— either because it had a LAT = 2, or because it failed the TOF or Y cuts, or if the residual kinetic energy of the muon at the C bank was < 100 MeV in the case of a C counter—those terms in the χ^2 involving the TOF and Y for that counter would be deleted and a penalty of four units was added to the muon χ^2. No muon candidates with LAT = 2 or bad TOF or Y information in more than one counter bank were retained.

The final choice of the best muon for an event was made on the basis of minimum muon χ^2. Other muon candidates were kept only if their χ^2 were within eight units of this minimum. The muon χ^2 distribution is shown in Fig. 9 for a sample of the data. No difference was observed between the muon χ^2 distributions for positive and negative tracks. Approximately 85% of all muons found

had good TOF and Y information in all three counter banks.

E. Selection of $K^0_{\mu 3}$ events

The events containing one or more muons were subjected to a vertex search, using every combination of a muon and another particle track. In addition, front tracks which were not correlated with any rear track to form a full particle track
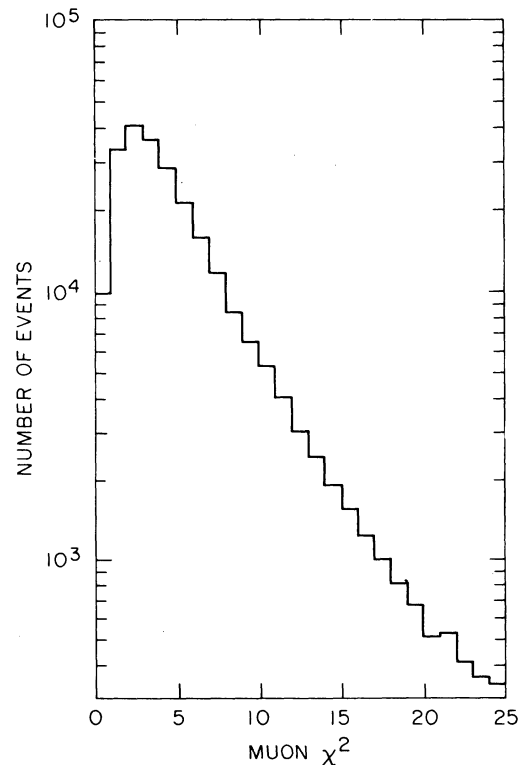

FIG. 9. Muon χ^2 distribution as obtained in the muon fitting scheme.

TABLE I. Event summary.

Events remaining through the various analysis states	Number of events (in thousands)
Events taken during acceptable running conditions	18 200
Events with reconstructable wire-chamber data	17 300
Events with sufficient tracks and counters	16 500
Events with identifiable muons	15 500
Events with a two-prong vertex in the decay volume	14 300

Events with identifiable muons are subdivided into event groups as described below		Number of events (in thousands)
Group	Description	
2 TRACK	Muon identification unambiguous, pion and muon seen in both chambers, vertex in decay volume	8452
1.5 TRACK	Muon identification unambiguous, pion not seen in downbeam chambers, vertex in decay volume	4701
NO PION	Muon identification unambiguous, no track verticizes with muon	1235
AMBIGUOUS	Muon identification ambiguous (either track could correlate with counters behind lead wall), vertex in decay volume	312
2 MUON	Two distinct muons present, both from common vertex in decay volume	193
MULTIPRONG	Muon identification unambiguous, more than two tracks share same vertex	244

were also used. The events were then grouped according to the result of this vertex search, as presented in Table I. The distribution in the square of the distance of closest approach for all combinations of tracks used in the vertex search is shown in Fig. 10 for a sample of the data.

The requirement for a prime event was that it contain one muon which formed a vertex with an upbeam track, assumed to be the pion. If the pion was observed in the downbeam chambers, and hence its momentum was measured, the event was placed in the 2 TRACK group. If the pion could not be located in the downbeam chambers, the event fell into the 1.5 TRACK group.

All other event groups were not included in the charge asymmetry sample, but were used to study systematic biases. The NO PION group contained events which had no tracks that formed a vertex with the muon. The AMBIGUOUS group had two muons which formed a vertex, but both were either correlated with the same pair of B and C counters, or triggered different counters in only one of the B and C banks. The 2 MUON events, on the other hand, had two muons emanating from a common
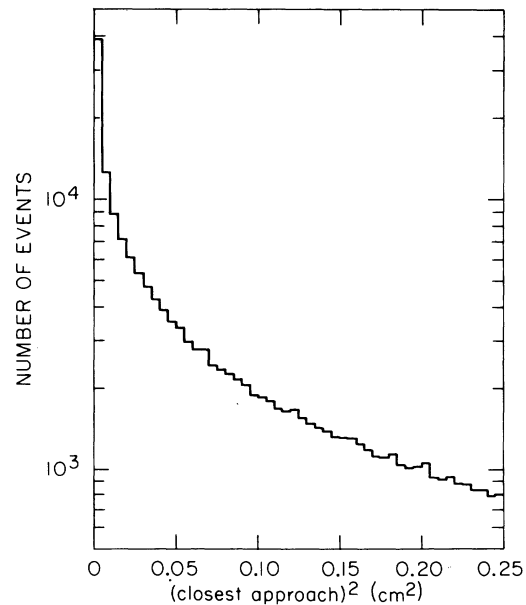

FIG. 10. Square of the distance of closest approach as observed in the search for a decay vertex in the beam volume. A cut was made at 50 cm².

decay vertex, triggering different counters in both the B and C counter banks. The MULTI-PRONG events appeared to have more than two tracks originating from a common vertex in the beam volume, with an unambiguous muon.

The details of events in each group were written onto a PASS-2 output tape. The information included the event group, the charge, momentum, upbeam direction, and counter information for each of the tracks which formed the decay vertex, as well as the location of the decay vertex itself.

F. K_L^0 momentum

The kaon TOF was computed for events in the 2 TRACK and 1.5 TRACK groups, which contained events with 2 and 1 rear tracks, respectively. In order to obtain the kaon TOF from the measured times, it was first necessary to subtract the difference between the transit times of the decay product and a direct $v \simeq c$ muon from the decay vertex to the timing counter. The corrected times for the A, B, and C counter banks for the tracks involved in the event were then assigned weights in the ratio 2:1:1, respectively, reflecting the timing accuracy obtainable in the respective counter banks. These were then averaged to give an over-all time for the kaon, representing the difference between the kaon TOF and the TOF for a $v \simeq c$ muon from the production target to the decay vertex. This value for the kaon TOF was also recorded on the PASS-2 output tape.

With the relationship $\Delta P_K / P_K = \gamma^2 [\Delta(\text{TOF}) / (\text{TOF})]$, where $\gamma = E_K / m_K$, the timing resolution of $\pm \frac{1}{3}$ nsec over a flight path of 75 m gave a K_L^0 momentum resolution of $\pm 2\%$ at $P_K = 2$ GeV/c, but only $\pm 25\%$ at $P_K = 7$ GeV/c.

VI. FINAL CUTS

The final stage of the analysis, PASS-3, involved the reading of event summaries off the PASS-2

output tapes. Various kinematic calculations were performed and numerous histograms were updated and stored on a disk. In addition, a set of final cuts was imposed at this stage of the analysis in order to reduce the level of certain contaminants in the data, as listed below (events which failed these cuts are presented in Table II; corrections for background remaining after these final cuts will be presented in Sec. VII):

(a) To avoid end-of-range effects for the muon, as discussed in Sec. VII C, events were cut if the computed residual muon energy at the C counter bank was less than 220 MeV.

(b) To reduce beam interaction contamination, as discussed in Sec. VII D, events were eliminated if the square of the transverse momentum of the muon was greater than 0.035 (GeV/c)^2. The kinematic limit for $K_{\mu 3}^0$ decays is 0.047 (GeV/c)^2.

(c) Since pion absorption effects become increasingly more pronounced with decreasing pion energy, events were cut if the kinematically fitted pion momentum could have been less than 500 MeV/c. Details of how this calculation was made are given in Sec. VII A. Monte Carlo studies indicated that this cut reduced the number of events with pion momentum < 500 MeV/c in our data sample by a factor of 10.

(d) Events in which the pion and muon fired the same T counter were eliminated since they were inconsistent with the trigger requirement. These events may have resulted through the presence of an additional T counter, either from accidentals or from the emission of a δ ray, or through erroneous assignment of both tracks to the same T counter in events where adjacent T counters were triggered. This class of events had a normal charge asymmetry, but was excluded in order to improve the agreement with the Monte Carlo events which were generated with 2 T's in the trigger.

(e) To exclude events resulting from beam

TABLE II. Asymmetries and number of events for each cut.

Event sample	Asymmetry in ppm	No. events in millions
2 TRACK and 1.5 TRACK events before cuts	$+3060 \pm 280$	13.15
(a) Events cut for low muon energy at C bank	-6120 ± 860	1.35
(b) Events cut for high muon transverse momentum	$+14320 \pm 1560$	0.41
(c) Events cut for fitted pion momentum	$+6370 \pm 690$	2.07
(d) Events cut for same pion and muon T counter	$+1810 \pm 1260$	0.63
(e) Events cut for vertex near T counter bank	-1080 ± 4770	0.04
(f) Events cut as possible $K_{\pi 3}^0$ candidates	$+3690 \pm 1520$	0.43
(g) Events cut for multiple C counters	$+7030 \pm 1400$	0.51
Events surviving all cuts		
2 TRACK	$+3360 \pm 440$	5.07
1.5 TRACK	$+2330 \pm 620$	2.63
Raw asymmetry δ_{raw}	$+3010 \pm 360$	7.70

interactions in the T counter bank, decay vertices were required to be at least 25 cm upbeam of the T bank.

(f) In order to reduce the magnitude of the correction for pion decay and pion penetration, as discussed in Sec. VII B, we endeavored to reduce the contamination due to $K_{\pi 3}^0$ events in our data by eliminating all events with a positive $P_0'^2$,[5] where

$$P_0'^2 = \frac{(m_K^2 - m_{+-}^2 - m_{\pi^0}^2)^2 - 4(m_{+-}^2 \, m_{\pi^0}^2 + m_K^2 \, P_\perp^2)}{4(P_\perp^2 + m_{+-}^2)},$$

in which m_{+-} represents mass of the (π^+, π^-) system, and $P_\perp$ its transverse momentum relative to the K_L^0 axis. Monte Carlo studies showed that this cut reduced the number of $K_{\pi 3}^0$ events in the data by a factor of 6.

(g) To reduce the number of events with possible hadronic penetration, primarily by pions, events with more than one C counter were eliminated. This cut required some consideration to ensure that it did not asymmetrically eliminate genuine events, and this is also discussed in Sec. VII B.

VII. SYSTEMATIC CORRECTIONS

The object of this experiment was to determine the intrinsic charge asymmetry in $K_{\mu 3}^0$ decay. The raw charge asymmetry, as determined from the 7.7 million events which passed all the cuts, is

$$\delta_{\text{raw}} = +3010 \pm 360 \text{ ppm}.$$

We were constrained, however, to perform our experiment in the presence of extraneous phenomena which affected the particles we studied and introduced systematic biases into the measurement. The identification and correction for these systematic biases is the most subtle aspect of the analysis.

Frequent references will be made to the results of the Monte Carlo studies made for this experiment. Since details of this program are given in paper II, we will only briefly outline the Monte Carlo studies here.

In order to make the Monte Carlo studies as realistic as possible, we have made use of experimentally observed distributions wherever possible. Moreover, in order that the Monte Carlo events be subjected to the same biases in the analysis programs, should there by any, the Monte Carlo output was in the form of raw spark and ADC information, written on tape in the same format as the data. These were then analyzed with PASS-1 and PASS-2, and subjected to the same set of cuts as used on the data in PASS-3. The advantage of this method lay in the parallel processing of experimental and Monte Carlo data, with a one-to-one correspondence in output histo-

grams which could easily be compared to look for systematic biases at every stage of the analysis.

A. Pion interactions

Hadronic interaction of pions was a major systematic bias. If a pion was absorbed or significantly scattered before it could be detected by the apparatus, the corresponding event was lost. If, furthermore, pions of one charge were preferentially lost, a systematic bias would result.

All pions that were fully detected in the experiment had to traverse two regions of material, each containing the same amount of matter. The upbeam section contained the decay-volume helium, the helium-bag wall, the T counter bank, and 10 wire-chamber planes. The downbeam section contained the magnet-volume helium, the helium-bag walls, a 3-mm-thick polystyrene sheet duplicating the mass and composition of the T bank, and 10 wire-chamber planes. Therefore, by measuring the pion loss in the downbeam section, we were able to compute the pion loss in the upbeam section and thereby determine the over-all asymmetry due to pion interactions.

The pion loss was found by kinematically selecting events from the 2 TRACK and 1.5 TRACK categories in which the pion was expected to traverse the magnet, and then determining the fraction of such events in which the pion was not observed downbeam. From the particle directions measured upbeam of the magnet, the muon momentum, the K_L^0 direction, and the particle masses, one may compute the pion momentum as a function of the kaon momentum. The locus of solutions for a sample event is shown in Fig. 11. From the event geometry, we computed the minimum pion momentum P_{min} necessary for the pion to traverse the magnet and still be detected in the downbeam chambers. Events in which the line $P_\pi = P_{\text{min}}$ lay below the closed curve could not have had a pion with momentum less than P_{min}, and hence should have had an observed downbeam pion. In a second class of events, the line $P_\pi = P_{\text{min}}$ intersected the curve at two kaon momenta $P_K^{(1)}$ and $P_K^{(2)}$, but the range in the K_L^0 momentum as determined from TOF was substantially higher than either $P_K^{(1)}$ or $P_K^{(2)}$, corresponding to solutions for the pion momentum that were greater than P_{min}. These events should also have had an observed downbeam pion.

The pion-loss analysis was carried out on 5.3 million events which had passed the final event cuts. Of these, 2 million were isolated by the kinematic selection procedure, and were expected to have downbeam pions. In this sample of selected events, 7.13% did not have a downbeam pion and were hence classified as pion-loss events; their
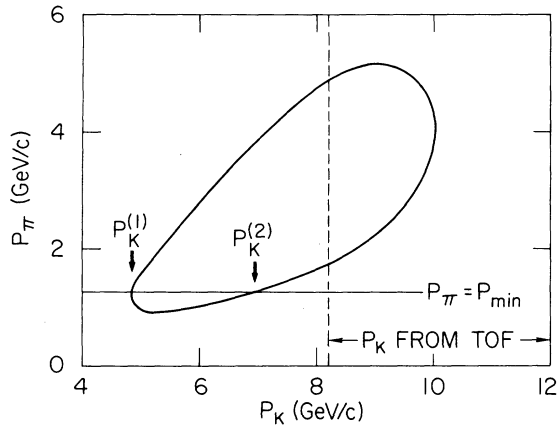
FIG. 11. Locus of solutions in the P_π-P_K plane for a sample event (see discussion in Sec. VII A). The range of P_K as determined from the TOF information is also shown.

muon charge asymmetry was $\delta_{loss} = -3390 \pm 2620$ ppm. This leads to a first-order correction for the pion loss in the upbeam section of

$$\delta_1 = (7.13 \pm 0.02\%)(\delta_{loss} - \delta_{raw})$$

$$= -456 \pm 188 \text{ ppm .}$$

The measured level of 7.13% pion loss was substantially higher than the expected hadronic absorption. However, we found through Monte Carlo studies that, because of measurement errors, the kinematic selection procedure failed to exclude all of the events in which the pion could not have traversed the magnet, leading to an apparent pion loss of 3.5%. Wire-chamber inefficiency and program reconstruction failures led to an additional apparent loss of 1.5–2.0%. The remaining 1.5–2.0% was attributed to hadronic absorption in the 0.86 g/cm² of material in the downbeam half of the apparatus. As only the product of the fraction lost and the charge asymmetry of lost events was important, the inclusion of charge-symmetric losses does not alter our final result.

This analysis suffered somewhat because the pion momentum spectrum downbeam of the magnet differed from that upbeam. Low-momentum pions were unlikely to traverse the magnet, and hence unlikely to contribute to the pion-loss analysis. As the pion absorption cross sections are the largest and most charge asymmetric at low momenta, this difference between the upbeam and downbeam pion momentum spectra could not be ignored. It was for this reason that the pion momentum cut, as discussed in Sec. VI, was made.

As described above, we were able to kinematically isolate events in which the pion momentum was above any given cutoff. We therefore excluded from our final data sample all events in which the

pion momentum might have been below 500 MeV/c. Note that this selection was made without reference to the downbeam pion track, if any. In addition, a second-order correction was applied to the remaining data, based on the observed charge asymmetry in the 2 TRACK events, to account for the difference in the momentum spectrum for the pion tracks observed in the downbeam chambers as opposed to that for pions observed in the upbeam chambers.

The final step in the pion-loss analysis was the determination of this second-order correction, δ_2. In computing δ_1, we selected events which should have had downbeam pions; let $f(P_\pi)$ be this selection probability for an event with pion momentum P_π. Had $f(P_\pi)$ been constant, δ_1 would have measured the pion absorption uniformly for all momenta. The correction δ_2 accounted for the variations in $f(P_\pi)$ from its mean value $\bar{f}$.

We obtained the differential pion absorption bias as a function of pion momentum by examining the asymmetry of the 2 TRACK events, assuming that its variation with pion momentum was due solely to the different amount of pion absorption as a function of pion momentum. As pions in the 2 TRACK events were required to traverse twice as much material as required of pions in prime events, the correction to be applied at pion momentum P_π is $\frac{1}{2}[\delta_{2\,TRK}(P_\pi) - \delta_{raw}]$, where $\delta_{2\,TRK}(P_\pi)$ is the measured asymmetry for pions with momentum P_π in the 2 TRACK events. If $\epsilon(P_\pi)$ is the fraction of all prime events with pion momentum P_π, then we have

$$\delta_2 = \sum_{P_\pi} \epsilon(P_\pi)[\bar{f} - f(P_\pi)]\frac{1}{2}[\delta_{2\,TRK}(P_\pi) - \delta_{raw}] .$$

The values of $\bar{f}$, $f(P_\pi)$, and $\epsilon(P_\pi)$ were determined from the Monte Carlo data, and are shown in Fig. 12. We found that $\delta_2 = +167 \pm 119$ ppm, leading to an overall correction for pion absorption of $\delta_1 + \delta_2 = -289 \pm 222$ ppm. A calculation of this correction based on πN cross sections is given in the Appendix.

B. Pion decay and penetration

Any process which might have caused an erroneous muon signature may have caused a systematic bias. Pion decay and pion penetration of the lead wall were two such processes.

The pion decay contamination was readily calculable. A series of Monte Carlo runs generated samples of $K_{\mu3}^0$, K_{e3}^0, and $K_{\pi3}^0$ decays with subsequent $\pi \to \mu\nu$ decays, which were then run through the same analysis programs as the real data. The fraction of events passing the final cuts from each initial mode, with the decay muon accepted as the best muon, determined the level of pion decay contamination in the real data. As the
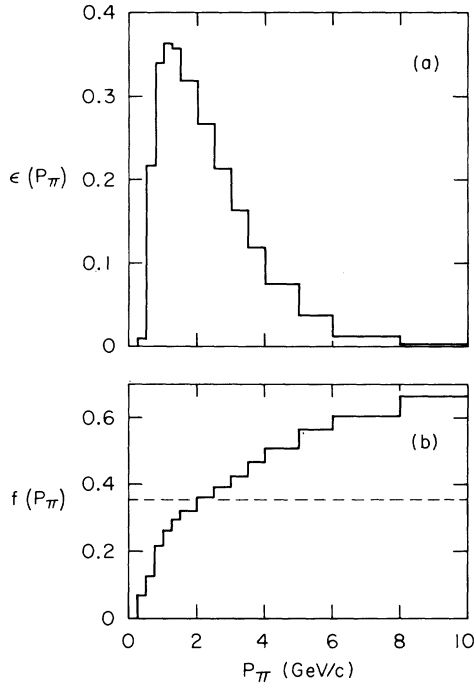
FIG. 12. The functional dependence of (a) $\epsilon(P_\pi)$ and (b) $f(P_\pi)$ on P_π, the laboratory pion momentum (see Sec. VII A for definitions of these functions). The broken line in (b) denotes the value of $\bar{f}$, the average value of $f(P_\pi)$.

pion decay process and the relative acceptances are well understood, this calculation should accurately duplicate the true level of pion decays in our data.

The correction to be applied for the decay mode i is $F_i(\delta_{\text{raw}} - \delta_i)$, where F_i is the fraction of events of mode i accompanied by pion decay included in the data sample, δ_i is the asymmetry for such pions, and δ_{raw} is the raw asymmetry measured in this experiment. Using the world average for the asymmetry in K_{e3}^0,[6] and our own measured asymmetry for the $K_{\mu3}^0$ events, we find the contributions from each mode to be

Mode i	δ_i (ppm)	F_i (%)	Correction (ppm)
$K_L^0 \to \pi^+\pi^-\pi^0$	0	0.51 ± 0.02	15 ± 1
$K_L^0 \to \pi^\pm e^\mp \nu$	-2996 ± 218	3.87 ± 0.11	$+232 \pm 18$
$K_L^0 \to \pi^\pm \mu^\mp \nu$	-3010 ± 360	2.95 ± 0.09	$+178 \pm 16$
Total		7.33 ± 0.15	$+425 \pm 24$

Before discussing the problem of pion penetration, a few words must be said about the cut involving events with more than one C counter, which was mentioned in Sec. VI as one method of reducing the number of events with possible pion

penetration in our data. A $K_{\mu3}^0$ event in which both the pion and the muon penetrated the lead wall could trigger two C counters. However, such events belong in the AMBIGUOUS or 2 MUON categories and were not included in the final data sample. A single muon could have physically traversed two C counters but this effect would have been charge-symmetric. Finally, there was the possibility of δ rays from a muon triggering adjacent C counters. δ-ray emission is charge-symmetric to first order, but could be charge-asymmetric in higher orders. The charge asymmetry as a function of the number of C counters triggered is shown in Fig. 13. The asymmetry for events with two C counters is 3300 ppm above the normal value. This difference may be due to hadronic penetration, in which case we would want to impose the $2C$ cut, or it may be due to δ-ray asymmetries, in which case the $2C$ cut would introduce a bias. Since the total asymmetry introduced by such events is only 130 ppm, we have decided to make the $2C$ cut and apply a correction of 65 ± 65 ppm to the charge asymmetry.

Our approach to the problem of events with pion penetration remaining in our data sample after the $2C$ cut was to isolate the $K_{\pi3}^0$ events in the data. Any asymmetry in these events must have been caused by the pion penetration process. We have computed the kinematic variable $P_0'^2$ for all 2 TRACK events in which the transverse momenta were compatible with $K_{\pi3}^0$ decay. Figure 14 shows the $P_0'^2$ distributions of the experimental data and the Monte Carlo data. The latter included events with pion decays from the $K_{\pi3}^0$, K_{e3}^0, and $K_{\mu3}^0$ decay
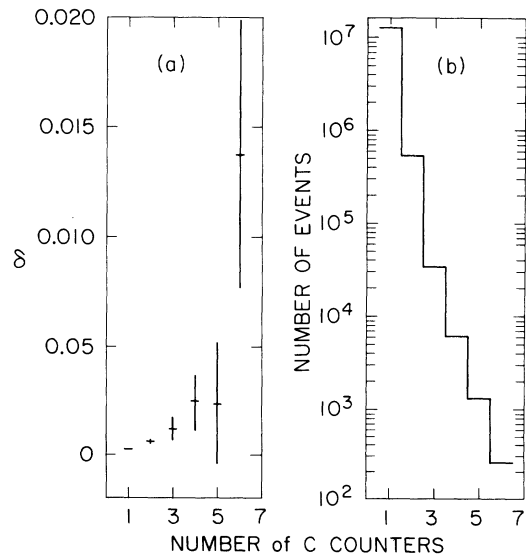

FIG. 13. (a) Charge asymmetry and (b) number of events as a function of the number of C counters triggered.
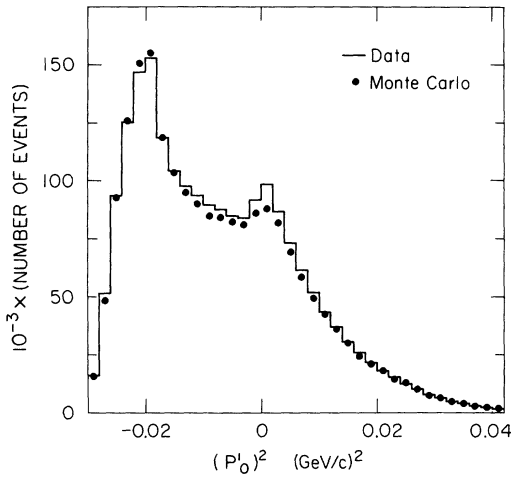
FIG. 14. $P_0'^2$ distribution for all 2 TRACK events in which the transverse momenta were compatible with $K_{\pi 3}^0$ decay. Both data and Monte Carlo are shown.

modes. The leptonic modes peak at negative values of $P_0'^2$, while the $K_{\pi 3}^0$ mode peaks at zero and should have positive values of $P_0'^2$ except for effects of experimental errors which result in some $K_{\pi 3}^0$ events with negative $P_0'^2$. The excess in the experimental data near $P_0'^2 = 0$ is indicative of pion penetration. Hence we endeavored to extract the pion penetration correction by studying events in the region $0 < P_0'^2 < 0.01$ $(\mathrm{GeV}/c)^2$, and subsequently extrapolating for all data via Monte Carlo.

We chose to calculate the product of the number of pion penetrations and their asymmetry because the error involved in the determination of this product was smaller than the errors involved in the separate evaluation of each term. In the selected $P_0'^2$ region, experimental events were assumed to consist only of $K_{\mu 3}^0$, $K_{\pi 3}^0$ with pion decay, and $K_{\pi 3}^0$ followed by pion penetration. The number of $K_{\mu 3}^0$ and K_{e3}^0 events with pion decay were small compared with the number of $K_{\mu 3}^0$ events with no pion decay, and were neglected in this analysis. Using the subscripts μ, π, and t to denote the contributions from $K_{\mu 3}^0$, $K_{\pi 3}^0$ with pion decay or penetration, and the sum of $K_{\mu 3}^0$ and $K_{\pi 3}^0$ decays, respectively, we have

$$N_t' = N_\mu' + N_\pi' ,$$

$$N_t' \, \delta_t' = N_\mu' \, \delta_\mu + N_\pi' \, \delta_\pi ,$$

where N denotes the number of events, and δ denotes the charge asymmetry. The prime superscript is a reminder that only events in the region $0 < P_0'^2 < 0.01$ $(\mathrm{GeV}/c)^2$ are involved; no primes are used in the terms involving δ_μ and δ_π since these asymmetries are assumed to be constant for all $P_0'^2$. Since pions came from all of the $K_{\pi 3}^0$, $K_{\mu 3}^0$, and K_{e3}^0 decay modes, and since our

estimate of the number of pions which might have contributed to pion penetration was based solely on the $K_{\pi 3}^0$ sample in a select $P_0'^2$ region, an enhancement factor g had to be determined by Monte Carlo methods:

$$g = N_\pi / N_\pi' ,$$

where N_π represents the number of all events with pion decay or penetration in the data sample, regardless of the value of $P_0'^2$. In addition, the fraction of events which were not $K_{\pi 3}^0$ in the selected sample,

$$r = N_\mu' / N_t' ,$$

was also determined by Monte Carlo. Since the experimental statistics in the selected band of $P_0'^2$ were poor, the uncertainty in the asymmetry observed in that region dominated any uncertainties introduced by the Monte Carlo. The charge asymmetry due to all events involving pion penetration in the entire data sample is thus

$$N_\pi \delta_\pi = g N_\pi' \delta_\pi$$

$$= g N_t' (\delta_t' - r \delta_\mu) .$$

Using the relationship

$$N \delta = N_\mu \, \delta_\mu + N_\pi \, \delta_\pi ,$$

where N and δ are the total number and charge asymmetry of all events in the final data sample, and N_μ the number of $K_{\mu 3}^0$ events in the same sample, we have

$$\delta_\mu = \frac{N\delta - N_\pi \delta_\pi}{N_\mu} \simeq \delta - g \left(\frac{N_t'}{N} \right) (\delta_t' - r \delta_\mu)$$

after making the approximation $N_\mu \simeq N$, since the number of pion-penetration events was small. The pion penetration correction is then given by

$$\delta_{\mathrm{pen}} = \delta_\mu - \delta$$

$$= - g \left(\frac{N_t'}{N} \right) (\delta_t' - r \delta_\mu) .$$

In order to allow for the fact that the pion-penetration problem varies with pion energy, we have divided the data into three pion-momentum bins, weighting the correction for each momentum bin by the number of events in that bin. The results are the following:

p_π (GeV/c)	N (10^3)	N_t' (10^3)	g	r	$\delta_t' - r\delta_\mu$ (10^{-4})	δ_{pen} (ppm)
< 4	6361	232	3.21	0.47	$+14 \pm 21$	-127 ± 191
$4-6$	1726	48	6.83	0.63	$+79 \pm 46$	-317 ± 185
> 6	92	2	9.21	0.75	-243 ± 227	$+55 \pm 51$

The combined result yields a pion-penetration correction of $\delta_{\mathrm{pen}} = -389 \pm 271$ ppm.

C. Muon interactions

Charge-asymmetric muon interactions in the lead wall would have biased the final result. Specifically, Coulomb scattering and range effects must be considered.

Coulomb scattering proceeding through one photon exchange must be charge-symmetric, but higher-order interference terms may be asymmetric. Figure 15 shows the charge asymmetry as a function of the observed scattering of the muon in traversing the lead wall. No variation was found and we have concluded that no correction was required.

Ionization differences between μ^+ and μ^- have been studied by Clark et al.[7] They observed that for a given initial energy, negative muons have a slightly longer range than positive muons. For the muons traversing our wall, we may expect an ionization difference of 3 MeV.

Finally, an end-of-range asymmetry exists as a result of μ^- capture. Neutrons produced by nuclear disintegration and X rays emitted during the muon cascade could effectively enhance the μ^- range by penetrating additional lead and then converting in the C counters.

We have examined our data for muon range differences, and show in Fig. 16 the charge asymmetry as a function of the computed energy of the muon at the C bank. A large negative asymmetry is apparent at the lowest muon energy, but the effect does not extend to higher energies. We have therefore discarded all events in which the computed muon energy at the C bank was less than

FIG. 16. Charge asymmetry as a function of the computed residual muon energy at the C counter bank. All events with $E_\mu < 220$ MeV are shown in the first bin, including events with muon energies apparently below the threshold required for penetrating the lead wall.

220 MeV in order to eliminate all possible biases due to end-of-range effects.

D. Beam interactions

Beam interactions with the helium nuclei in the decay volume could to some extent simulate $K_{\mu 3}^0$ decays. To measure this effect, we have made several data runs with a 2.5-cm-thick carbon slab in the beam, placed successively at seven different positions along the beam line in order to obtain a uniform measure of the interaction bias. Carbon was chosen because it is a spin-0 nucleus with equal numbers of protons and neutrons, as is helium. Assuming that the number of interactions increases as $A^{2/3}$, the carbon data should have produced 29 times as many interactions as contained in all of the helium data. As we restricted our attention here to events originating from the slab itself, the effects of regeneration were not considered. A separate discussion of regeneration is given in Sec. VII G.

From the carbon data, the muon transverse momentum distribution for interaction events was observed to extend to very high values, as shown in Fig. 17. We have therefore imposed a muon transverse momentum cut on the primary data, requiring $P_{\mu \perp}^2 < 0.035$ $(\text{GeV}/c)^2$. Figure 18 shows the vertex distributions before and after the final cuts, for events from the carbon run with the carbon slab at two different positions along the beam line.

Our analysis indicated that the level of interactions was very low. The trigger rate was increased only 3% by the presence of the carbon slab. From the excess of events near the slab, we were able to determine the fraction of events in the data
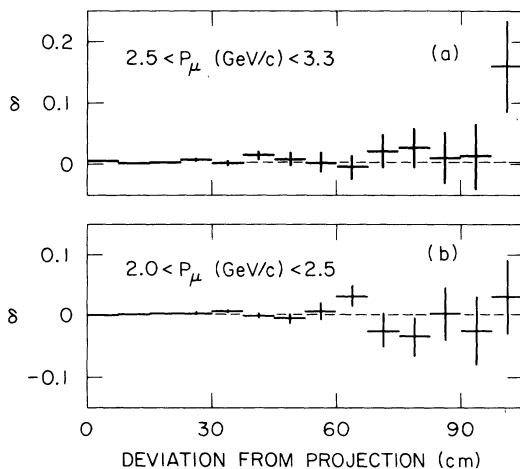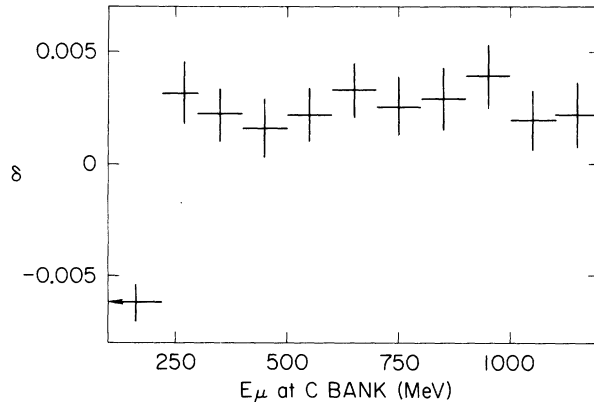

FIG. 15. Charge asymmetry as a function of muon scattering in the lead wall for (a) $2.5 < P_\mu < 3.3$ and (b) $2.0 < P_\mu < 2.5$ GeV/c in the laboratory. The broken lines indicate our value for the raw asymmetry, δ_{raw}. The abscissa measures the horizontal displacement between the projected X position of the muon trajectory at the C bank and the center of the associated C counter.
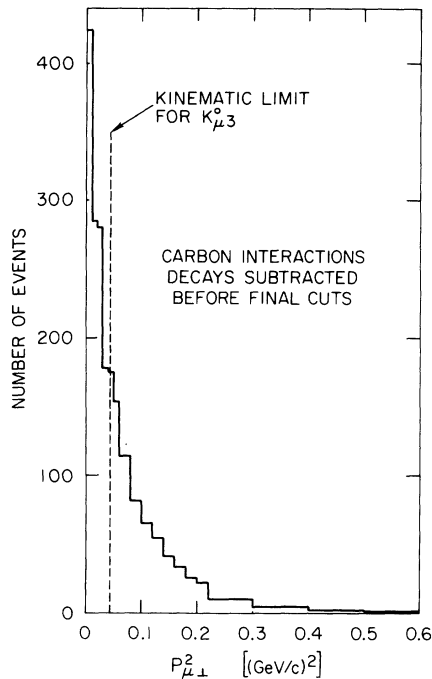
FIG. 17. Number of events as a function of the square of the muon transverse momentum for data collected in the carbon runs. The corresponding spectrum for decays observed in regular helium runs has been subtracted. The data are shown here before final cuts.

which were attributed to interactions in the carbon. This fraction, together with the observed change in the charge asymmetry for events near the slab, enabled us to compute the correction for interaction contamination for any particular
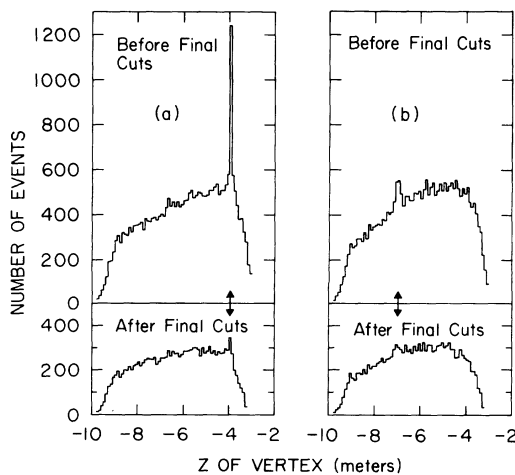

FIG. 18. Number of events as a function of the Z position of the decay vertex, before and after final cuts, for runs with a 2.5 cm carbon slab at (a) $Z = -4m$ and (b) $Z = -7m$, as indicated by the arrows. $Z = 0$ is at the center of the spectrometer magnet.

carbon run. The correction to the main data sample was then obtained by averaging the effects from each slab position, and dividing by the carbon/helium enhancement factor. The results are

Fraction of interactions in carbon data

$$= (0.49 \pm 0.05)\%,$$

Asymmetry of interaction events $= (-5.0 \pm 11.0)\%$,

Carbon slab/helium enhancement factor $= 29$,

Correction for beam interaction $= +8 \pm 19$ ppm.

E. Muon charge ambiguities

Any ambiguity in the determination of the muon charge would have diluted our measured asymmetry. Since particle deflections in the magnet (19 mrad for 20-GeV/c particles) were much greater than our 1 mrad angular resolution, the charge of each particle was determined unambiguously. There were some events, however, in which there were more than one muon candidate. These events were placed in the AMBIGUOUS or 2 MUON groups if the best candidate was not at least three standard deviations better than all others, and these event groups were not included in the charge asymmetry computation.

The only remaining concern was that more events of one charge combination than the other might have fallen into the AMBIGUOUS group. We found that 0.23% of all events falling in the AMBIGUOUS group had two B counters and one C counter. These events were most likely due to a pion penetrating to the B bank, triggering a second B counter in proximity to the B counter triggered by the real muon. Although the pion did not trigger a C counter, it was nevertheless misidentified as a muon with the use of the muon C counter. The charge asymmetry observed in the 2 TRACK events with pions that penetrated to the B bank but not the C bank was $(+2.07 \pm 0.37)\%$. As there could thus be a bias in excluding the AMBIGUOUS events with two B counters and one C counter, a correction of -25 ± 25 ppm was applied.

F. Geometric asymmetries

If the detection efficiency were different for positive and negative muons, a systematic bias would have resulted. Geometric asymmetries in the apparatus would have resulted in such a bias if positive muons, for example, always hit the same side of the detector. By taking equal amounts of data with each of the two magnet polarities (forward and reverse), and then computing the charge asymmetry as

$$\delta = \frac{r-1}{r+1},$$

where

$$r = \left(\frac{N_+ \uparrow\, N_+ \downarrow}{N_- \uparrow\, N_- \downarrow}\right)^{1/2} ,$$

$N_+ \uparrow$ = number of μ^+ events with magnet polarity forward, etc., the effects of constant geometric asymmetries were completely eliminated. We have verified this by considering various subsets of the data in which widely varying geometrical asymmetries were artificially introduced by successively subtracting the events involving counters $C1$, $C2$, etc. As seen in Fig. 19, the charge asymmetry shows no variation with the artificially generated geometric asymmetries.

We have also examined the data for time-varying geometric asymmetries, such as might be caused by gradual changes in wire-chamber efficiency. Consecutive data runs with opposite magnet polarities were paired, and the charge asymmetry was computed for each of 169 such pairs. The χ^2 for the hypothesis of a constant asymmetry was 178 for 168 degrees of freedom, corresponding to a confidence level of 27%.

G. Regeneration

When a K_L^0 beam traverses material, the K^0-$\overline{K}^0$ mixture is altered by coherent regeneration. This is equivalent to changing the CP-mixing parameter ϵ, thus introducing a small systematic bias.

Consider the regeneration in the veto counter V. The coherent regeneration amplitude as a function of distance after a thin regenerator is given by[8]

$$A(Z) = if_{21} \lambda\, NL \exp[(i\delta - 1/2)\, Z/\Lambda] ,$$

where

f_{21} = half the difference between the K^0 and $\overline{K}^0$ forward scattering amplitudes,
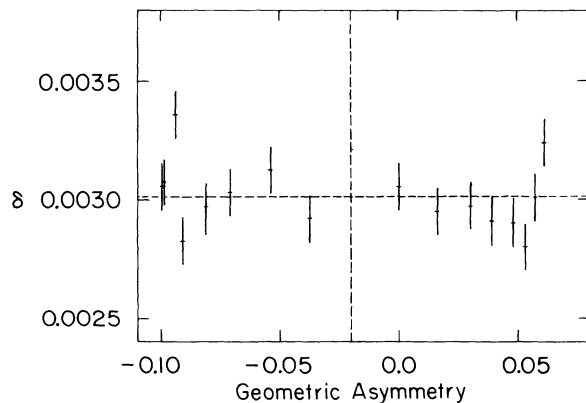

FIG. 19. Charge asymmetry as a function of the geometric asymmetry introduced by eliminating each of the 16 C counters in turn. The horizontal and vertical broken lines indicate the raw charge asymmetry and the geometrical asymmetry for all the data, respectively.

$\lambda = K_L^0$ wavelength,

N = density of nuclei,

L = thickness of regenerator,

$\delta = K_L^0$, K_S^0 mass difference in units of K_S^0 lifetime,

Z = distance downbeam of the regenerator,

$\Lambda = K_S^0$ mean decay length.

From the data of Abrams et al.[9] and Bott-Bodenhausen et al.,[10] we found that $|A(0)| = 3 \times 10^{-4}$, and that the total correction required was -12 ± 6 ppm.

Consider now the effect of the helium in the decay volume. Within a diffuse regenerator, the coherent amplitude attains a constant value of

$$A = if_{21}\, N\lambda\Lambda/(\tfrac{1}{2} - i\delta)$$

after the first few K_S^0 mean decay lengths. Extrapolating the helium parameters from the carbon data, we found that helium regeneration led to a correction of -4 ± 2 ppm. Incoherent regeneration is an even smaller contribution and can be neglected.

H. Pulse-height variation

Slight variations in the mean pulse heights recorded in the counters were observed between the magnet-forward ($\uparrow$) and the magnet reverse ($\downarrow$) data. We have shown in Fig. 20 the pulse-height spectra for $C15$, the counter in which this effect was greatest. The mean $\uparrow$ pulse height was 0.54% greater than the mean $\downarrow$ pulse height. As
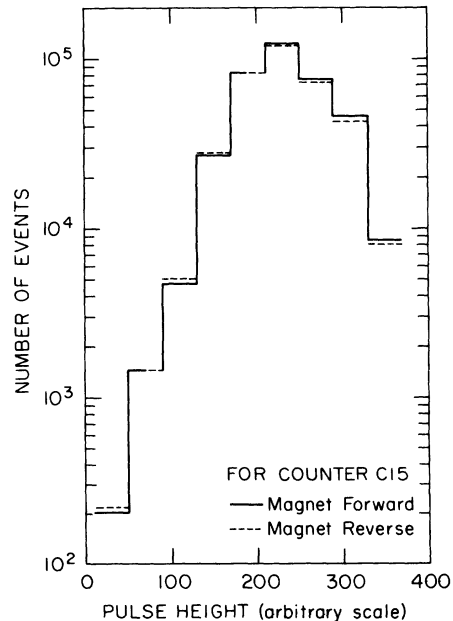

FIG. 20. Pulse-height distribution as a function of forward and reverse magnetic field for counter $C15$.

C15 was on the left edge of the C bank, only μ^+'s hit it for magnet ↑, and μ^-'s for magnet ↓. Thus the μ^- pulse heights were effectively attenuated by 0.54%, and more μ^-'s would have failed to trigger $C15$ than μ^+'s. Since the thresholds for all discriminators used on counter phototubes were low, corresponding typically to 15% of the pulse height for a minimum ionizing particle, few events were affected. From the number of events per ADC count at threshold, and the fractional shifts in the μ^+ and μ^- spectra, we have computed the bias introduced for each counter. Summing over all counters, the total correction is found to be −2 ±2 ppm.

I. Accidentals

Accidentals are a major concern at an accelerator with a poor duty cycle. Background tracks and scintillation counters may be accidentally correlated by the analysis programs, generating spurious events. Our two major concerns are in the identification of muons and in the vertex search.

In the identification of muons, there were many constraints as evidenced by the terms in the χ^2 defined in Sec. V D. We expect the χ^2 distribution of accidental muons to extend to higher values than that of the real muons. Hence, if a bias were introduced, it would be evident at high muon χ^2 values where the accidentals would be relatively more abundant. Upon examining the charge asymmetry as a function of the muon χ^2, we found that the hypothesis of constant asymmetry fitted the data with a 97.5% confidence level.

Accidental vertex formation was more worrisome since there was a charge-asymmetric background of uncorrelated muons tracks, and there was only one constraint to provide discrimination. This bias was studied by taking these lone muons, which had no vertex with any other track, and pairing them with pion tracks from separate events which had formed vertices with muons, and were known to have come from $K^0_{\mu 3}$ decays. If the pair happened to form an acceptable vertex, it was subjected to all the normal event-selection criteria. We found that 790 ±10 ppm of our events could be attributed to accidental vertex formation, and that the asymmetry of such events was (+1.0 ±1.3)%, leading to a correction of −8 ±10 ppm.

J. General checks

We have made corrections for all the systematic biases that we have been able to isolate, and these corrections are tabulated in Table III. Although we can never be completely certain that no additional biases exist, we can reduce the chance of substantial error by a thorough examination of

TABLE III. Tabulation of systematic corrections and final charge asymmetry.

Description	Absolute corrections
Events passing final cuts	+3010±360 ppm
Pion absorption	−289±222
Pion decay	+425±24
Pion penetration	−389±271
Beam interactions	+8±19
Pulse height variation	−2±2
Asymmetric contributions to AMBIGUOUS event group	−25±25
Asymmetric elimination of multiple C counter events	+65±65
Regeneration	−16±6
Accidentals	−8±10
Final charge asymmetry	+2779±508 ppm

the data. Should a sizable bias exist in the data, we could reasonably expect that it would affect certain subsets of the data more than others.

In this spirit, we have examined the asymmetry as a function of many variables, including such physically important parameters as the particle momenta in the laboratory, the counters which triggered, and the decay vertex position. The intrinsic asymmetry should be constant, and a χ^2 and the number of degrees of freedom for the hypothesis of a constant asymmetry were calculated for each distribution. *We emphasize that the known biases discussed previously have not been subtracted from these distributions.*

Figure 21 shows the asymmetry as a function of the momentum of the muon and the pion in the laboratory. The muon distribution shows no dependence. The pion distribution suffers from a substantial deviation ($\chi^2 = 11$) in the region 0.5–1.0 GeV/c. This is precisely the region of maximum differential pion absorption where we expect the measured asymmetry to be reduced, although the magnitude of the effect is larger than expected.

Figure 22 shows the asymmetry as a function of the muon counters. To compute this distribution, we have combined the data from symmetrically positioned counters, and computed the asymmetry for each such pair. All distributions are adequately consistent with no variation in the asymmetry.

Figure 23 shows the asymmetry as a function of the Z position of the decay vertex; again no variation is apparent. Since the helium bag was much larger than the cross section of the beam, we had no reason to suspect contamination at the X or Y edges of the decay volume, and none was found.
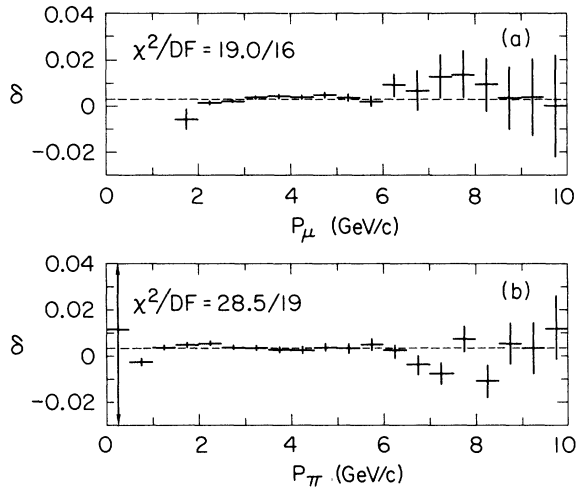
FIG. 21. Charge asymmetry as a function of the laboratory momentum of the (a) muon and (b) pion. The broken line in each plot indicates our value for δ_{raw}.

VIII. RESULTS AND CONCLUSIONS

Our final value for the charge asymmetry in $K_L^0 \rightarrow \pi^{\mp}\mu^{\pm}\nu$ decay is $\delta_\mu = (2.78 \pm 0.51) \times 10^{-3}$, which is in reasonable agreement with previous determinations of δ_μ and δ_e, as summarized in Table IV. The good agreement between δ_μ and δ_e reinforces the concept of μ-e universality, and indicates the absence of substantial (real or imaginary) $\Delta S = -\Delta Q$ amplitudes and T violation due to electromagnetic final-state interactions. As an additional test of these concepts, we have plotted in Fig. 24 the (uncorrected) charge asymmetry as a function of E_π, E_μ, and E_ν on the Dalitz plot. A real g_+ or g_- would result in variation of δ with E_π, whereas a pure imaginary g_+ or g_- would result in variation of δ_μ with both E_π and E_μ. An imaginary part of the $\Delta S = \Delta Q$ form factors f_+ and f_- would cause variation of δ_μ with $\cos\theta = \vec{P}_\mu \cdot \vec{P}_\nu$. It should also be noted that CPT invariance is sufficient to ensure that the effects of all electromagnetic final-state interference terms vanish when properly weighted across the Dalitz plot. To the statistical level of the present experiment, we see no significant variation in δ_μ in any projection of the Dalitz plot. With present limits on $\Delta S = -\Delta Q$ amplitudes and on $\text{Im}\xi$, however, one would not expect such effects to be observable with less than $\sim 10^8$ events.[2]

If we assume that there are no $\Delta S = -\Delta Q$ amplitudes, i.e., that $x = 0$, then the result of this experiment is $\text{Re}\epsilon = (1.39 \pm 0.25) \times 10^{-3}$. Assuming further that CP violation in the K^0-$\bar{K}^0$ system is due solely to the nonorthogonality of the decay eigenstates, as in the superweak theory,[11] then one expects $\eta_{+-} = \eta_{00} = \epsilon$. The latest Particle Data
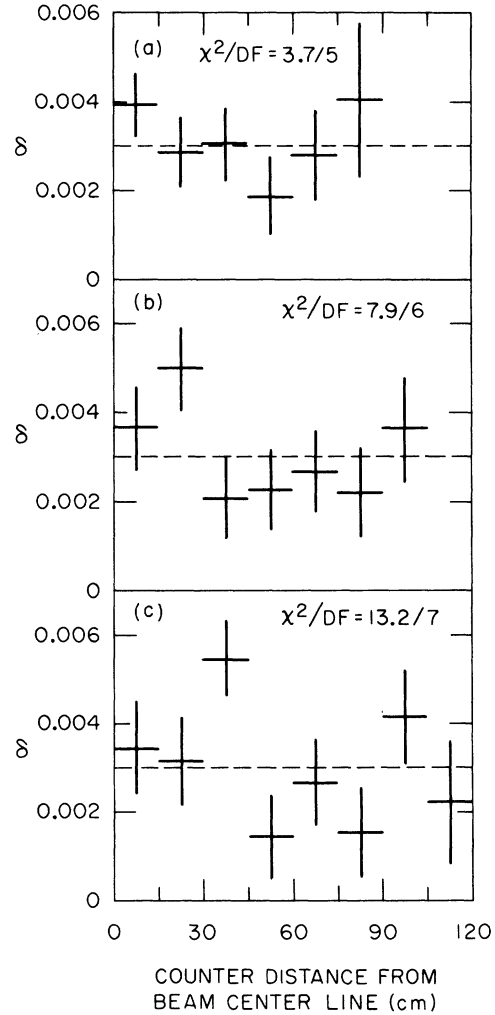

COUNTER DISTANCE FROM
BEAM CENTER LINE (cm)

FIG. 22. Charge asymmetry as a function of the horizontal displacement from the beam center line at the (a) A, (b) B, and (c) C counter banks. The broken lines indicate our value for δ_{raw}.
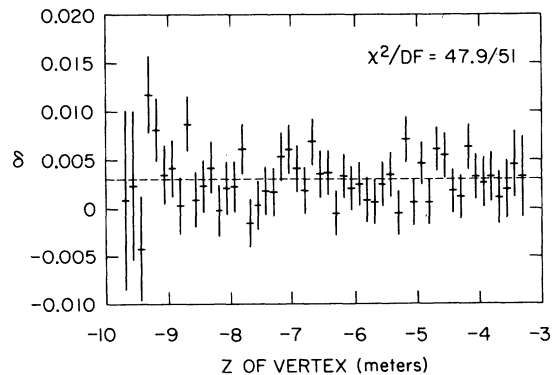

Z OF VERTEX (meters)

FIG. 23. Charge asymmetry as a function of the Z position of the decay vertex. The broken line indicates our value for δ_{raw}.

TABLE IV. Charge asymmetry in K_{l3}^0 decay.

δ_e		δ_μ	
Experiment	$10^3\delta_e$	Experiment	$10^3\delta_\mu$
Saal *et al.* (Ref. 6)	2.46 ± 0.59	Dorfan *et al.*[a]	4.03 ± 1.34
Marx *et al.* (Ref. 6)	3.46 ± 0.33	McCarthy *et al.*[b]	6.0 ± 1.4
Ashford *et al.* (Ref. 6)	3.6 ± 1.8	This experiment	2.78 ± 0.51
Webb *et al.* (Ref. 6)	2.66 ± 0.34		
Average	$10^3\delta_e = 3.00 \pm 0.25$	Average	$10^3\delta_\mu = 3.26 \pm 0.45$

$\chi^2 = 3.9$ for 3 degrees of freedom. $\chi^2 = 5.0$ for 2 degrees of freedom.

$$\delta_l = (3.05 \pm 0.24) \times 10^{-3}$$

$\chi^2 = 9.2$ for 6 degrees of freedom.

[a] D. Dorfan, J. Enstrom, D. Raymond, M. Schwartz, S. Wojcicki, D. H. Miller, and M. Paciotti, Phys. Rev. Lett. 19, 987 (1967).

[b] R. L. McCarthy, J. H. Brewer, R. J. Budnitz, A. C. Entis, R. M. Graven, D. H. Miller, and W. N. Ross, Phys. Lett. 42B, 291 (1972).

Group average for $|\eta_{+-}|$ is $(1.98 \pm 0.04) \times 10^{-3}$.[12] This does not include the recent measurement by the Colorado–U. C. Santa Cruz–SLAC collaboration[13] of $|\eta_{+-}| = (2.23 + 0.05) \times 10^{-3}$. The Particle Data Group value for direct measurements of $|\eta_{00}|$ is $(2.09 \pm 0.10) \times 10^{-3}$, while the two most recent experiments yield $|\eta_{00}| / |\eta_{+-}| = 1.013 \pm 0.046$.[12] Assuming the "natural phase" of 43.6° for η_{+-} and η_{00}, our experiment yields $|\epsilon| = (1.92 \pm 0.35) \times 10^{-3}$, while the world average of charge asymmetry experiments gives $|\epsilon| = (2.10 \pm 0.17) \times 10^{-3}$. Thus, the present experimental situation, while it contains some uncertainties in both $|\eta_{+-}|$ and $|\eta_{00}|$, is consistent with the hypothesis that the source of CP violation in K^0 decays is in the mass

matrix.

Finally, if we use the value of $\mathrm{Re}\,\epsilon$ from the $K_{\pi 2}^0$ experiments, we may obtain a value for $\mathrm{Re}\,x$. With the Colorado–U.C. Santa Cruz–SLAC value for $|\eta_{+-}|$, and using $\theta_{+-} = 43.6°$, the assumption $\eta_{+-} = \epsilon$ leads to

$$\mathrm{Re}\,\epsilon = |\eta_{+-}| \cos\theta_{+-} = (1.6 \pm 0.03) \times 10^{-3}.$$

Consequently, we find

$$\frac{1 - |x|^2}{|1 - x|^2} = \frac{\delta_\mu}{2\,\mathrm{Re}\,\epsilon} = 0.87 \pm 0.16.$$

Assuming that x is small,[14] this reduces to

$$|1 - x| = 1.07 \,^{+0.12}_{-0.09},$$

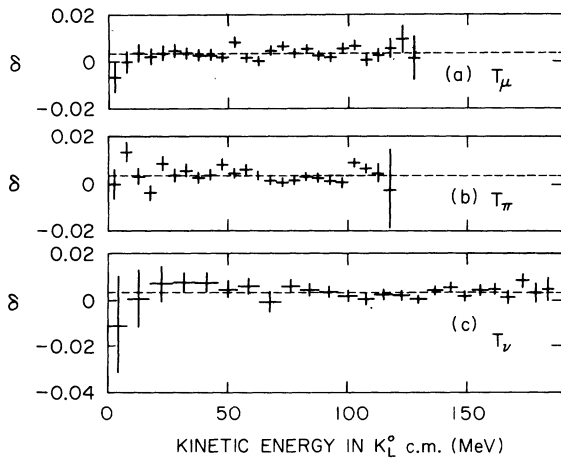giving $\mathrm{Re}\,x = 0.07 \,^{+0.09}_{-0.12}$.

FIG. 24. Charge asymmetry as a function of the center-of-mass kinetic energy of the (a) muon, (b) pion, and (c) neutrino. The broken lines indicate the best fit to a constant, giving a χ^2 of (a) 23.6 for 25 D.F. (degrees of freedom) (b) 36.7 for 23 D.F., and (c) 22.7 for 24 D.F. None of the fits were significantly improved by the inclusion of linear or quadratic terms.

APPENDIX: CALCULATION OF CORRECTION FOR PION ABSORPTION

We present here a simple, first-order calculation for the correction for the absorption of pions from $K_{\mu 3}^0$ decay in the upbeam section of the spectrom-

eter. We will neglect the finer details of nuclear structure and diffractive scattering and consider only πN scattering. All pions which interact in the material will be considered to be lost. In addition, the laboratory pion momentum spectrum for the 1.5 TRACK events, which was not measurable in the experiment, is inferred from the Monte Carlo study.

The amount of material present in the upbeam section of the spectrometer was 0.86 g/cm^2, consisting of 0.32 g/cm^2 in the T scintillation counters, 0.16 g/cm^2 in the copper wires of the wire spark chambers, 0.06 g/cm^2 in the Mylar windows, and 0.32 g/cm^2 in the helium and neon gas. Since the total $(\pi^+ p) + (\pi^+ n)$ and $(\pi^- p) + (\pi^- n)$ cross sections are expected to be equal on the basis of isotopic spin, the only material that could give rise to differential pion absorption is the excess of protons in the scintillator and the Mylar, and the excess of neutrons in the copper wires, being 0.027 g/cm^2 of protons and 0.014 g/cm^2 of neutrons, respec-

tively. This is a net of 0.013 g/cm^2 of proton excess in all of the material in the upbeam section of the spectrometer which may contribute to pion absorption.

Using the $(\pi^+ p)$ and $(\pi^- p)$ differential total cross sections[15] integrated over the laboratory pion momentum spectrum for the 2 TRACK and 1.5 TRACK events (after requiring pion momentum > 500 MeV/c), we find the average value of $\sigma_{tot}(\pi^- p)$ $- \sigma_{tot}(\pi^+ p)$ to be 7 ± 1 mb. This corresponds to a muon charge asymmetry of $- 55 \pm 8$ ppm in those $K_{\mu 3}^0$ events which had a pion absorbed in the upbeam section of the spectrometer. Since such events were not included in our final sample of events that was used to compute the charge asymmetry δ_{raw}, this correction of $- 55 \pm 8$ ppm must be added to δ_{raw}.

The corresponding correction for pion absorption was determined experimentally to be $- 289 \pm 222$ ppm (Sec. VII A), which is in fair agreement with the value calculated above.

---

†Work supported by the U. S. Atomic Energy Commission.

‡Present address: Weizmann Institute of Science, Rehovoth, Israel.

§Present address: Rockefeller University, New York, New York 10021.

‖Alfred P. Sloan Foundation Fellow.

[1]An earlier report of this experiment has been given by R. Piccioni, R. Coombes, G. Donaldson, D. Dorfan, D. Fryberger, D. Hitlin, J. Liu, R. Messner, B. Meyer, D. Porat, A. Rothenberg, M. Schwartz, D. Uggla, and S. Wojcicki, Phys. Rev. Lett. 29, 1412 (1972).

[2]J. C. Brodine, Nucl. Phys. B30, 545 (1971); J. S. Bell and R. K. P. Zia, ibid. B17, 388 (1970); C. Ryan, Phys. Rev. D 1, 299 (1970).

[3]G. W. Brandenburg, W. B. Johnson, D. W. G. S. Leith, J. S. Loos, G. J. Luste, J. A. J. Matthews, K. Moriyasu, W. M. Smart, F. C. Winkelmann, and R. J. Yamartino, Phys. Rev. D 7, 708 (1973).

[4]R. Coombes, D. Fryberger, D. Hitlin, R. Piccioni, D. Porat, and D. Dorfan, Nucl. Instrum. Methods 98, 316 (1972).

[5]The variable $P_0'^2$, which is computed assuming the decay is a $K_{\pi 3}^0$ decay, is positive for $K_{\pi 3}^0$ and negative for K_{l3}^0 decays, in the absence of measurement errors. This variable was first used by A. Astier, L. Blaskovic, M. M. DeCourreges, B. Equer, A. Lloret, P. Rivet, and J. Siaud, in Proceedings of the Aix-en-Provence Conference on Elementary Particles, 1961 (Centre d'Etudes Nucléaires de Saclay, Gif-sur-Yvette, Seine et Oise, Saclay, France, 1961), p. 227. (This work is available in English as SLAC-Trans-143.)

[6]We have taken an average charge asymmetry for K_{e3}^0 to be $(+ 3.00 \pm 0.25) \times 10^{-3}$, based on the results of H. Saal [Columbia Univ. Report No. Nevis-169, 1969

(unpublished)], J. Marx, D. Nygren, J. Peoples, T. Kirk, and J. Steinberger [Phys. Lett. 32B, 219 (1970)], V. A. Ashford, B. C. Brown, G. E. Masek, T. Maung, E. S. Miller, H. Ruderman, D. J. Shields, and W. Vernon [ibid. 38B, 47 (1972)], and R. C. Webb, thesis, Princeton Univ. Technical Report No. 3, 1972 (unpublished).

[7]A. R. Clark, T. Elioff, R. C. Field, H. J. Frisch, R. P. Johnson, L. T. Kerth, and W. A. Wenzel, Phys. Rev. Lett. 26, 1667 (1971).

[8]W. A. W. Mehlhop, S. S. Murty, P. Bowles, T. H. Burnett, R. H. Good, C. H. Holland, O. Piccioni, and R. A. Swanson, Phys. Rev. 172, 1613 (1968).

[9]R. J. Abrams, R. L. Cool, G. Giacomelli, T. F. Kycia, B. A. Leontić, K. K. Li, A. Lundby, D. N. Michael, and J. Teiger, Phys. Rev. D 4, 3235 (1971).

[10]M. Bott-Bodenhausen, X. de Bouard, D. Dekkers, R. Felst, R. Mermod, I. Savin, P. Scharff, M. Vivargent, T. R. Willitts, and K. Winter, Phys. Lett. 24B, 438 (1967).

[11]L. Wolfenstein, Phys. Rev. Lett. 13, 562 (1964).

[12]Particle Data Group, Rev. Mod. Phys. 45, S1 (1973).

[13]R. Messner, R. Morse, U. Nauenberg, D. Hitlin, J. Liu, R. Piccioni, M. Schwartz, S. Wojcicki, and D. Dorfan, Phys. Rev. Lett. 36, 876 (1973).

[14]K. Winter, Rapporteur's talk, in Proceedings of the Amsterdam International Conference on Elementary Particles, 1971, edited by A. G. Tenner and M. Veltman (North-Holland, Amsterdam, 1972); G. Burgun, E. Lesquoy, A. Muller, E. Pauli, S. Zylberajch, F. James, L. Montanet, E. Paul, P. Saetre, D. M. Sendall, and O. Skjeggestad, Nuovo Cimento Lett. 2, 1169 (1971).

[15]E. Flaminio, J. D. Hansen, D. R. O. Morrison, and N. Tovey, CERN Reports Nos. CERN/HERA 70-5 and 70-7, 1970 (unpublished).